



The effects of rib shape and slit on fatigue properties of orthotropic steel decks

Koichi Yokozeki¹ · Tomonori Tominaga¹ · Chitoshi Miki²

Received: 19 February 2018 / Accepted: 6 November 2020 / Published online: 16 November 2020
© International Institute of Welding 2020

Abstract

Orthotropic steel decks are composed of comparatively thin steel plates (as thin as 6 mm) that deform in the in-plane and out-of-plane directions at longitudinal-to-transverse rib connections in response to vehicle loads. Since such deformations can change as the load positions move, local stress directions can also vary such that hot spots along the weld toes are moved and the relationship between the load position and hot spot stress becomes complex. Furthermore, the deformations will differ depending on the specific type of connection. The present work investigated the effects of rib shapes and slits (that is, cut-outs) on the fatigue properties of such connections by calculating structural hot spot stresses at various connections by finite element analyses. The hot spot locations along weld toes were determined to vary depending on the load position, the longitudinal rib shape, and the presence of slits. It was also found that the load positions associated with maximum and minimum hot spot stresses at slit connections tended to be eccentric relative to the center axes of the evaluated ribs.

Keywords Structural members · Bridges · Fatigue strength · Computation · Stress analysis · Weld toes

1 Introduction

Orthotropic steel decks are lightweight compared to concrete decks and are used in many long-span bridges and urban expressways. These steel decks are also used in the rehabilitation of bridges by replacing deteriorated concrete decks, and the demand for these structures is increasing [1]. However, numerous fatigue cracks have been detected in orthotropic steel decks [2, 3], especially at connections between longitudinal and transverse ribs. As an example, inspections of urban expressways in Japan have found close to 10,500 cracks, approximately 40% of which appeared at longitudinal-to-transverse rib connections [4]. Although several different connection types have been developed in previous studies [5–8], all such designs continue to exhibit fatigue cracks.

Orthotropic steel decks are composed of comparatively thin, flexible steel plates (as thin as 6 mm) and are directly

subjected to vehicle loads. These plates are readily deformed in the out-of-plane direction [9], such as via torsion and distortion of the ribs [10, 11]. The deformed longitudinal and transverse ribs are constrained by one another at the connections, and this induces three-dimensional in-plane and out-of-plane deformations of the ribs. Since such deformations can change as the load positions move, the local stress directions can also change such that the stress concentration points (that is, the hot spots) migrate along the weld toes [12]. As an example, one possible hot spot is located at the side of the box weld at the joint between a U-rib and a slit transverse rib and appears in the case that a longitudinal in-plane tension acts on the U-rib. However, the hot spot transfers to the base of the box weld when the out-of-plane bending about the longitudinal axis acts on the U-rib wall (Fig. 1). Because the deformations of longitudinal-to-transverse rib connections can change as the load position moves, hot spots are not fixed points.

The deformation changes produced by moving load positions can generate complex relationships between load positions and hot spot stresses (hereinafter referred to as an influence surface) at the longitudinal-to-transverse rib connections. It has also been determined that the load positions that maximize the hot spot stresses can be situated some distance from the center axes of the ribs [13, 14]. In addition, the actual vehicle positions can migrate in the longitudinal and transverse directions [15]. Therefore, it is vital to consider the load

Recommended for publication by Commission XIII - Fatigue of Welded Components and Structures

✉ Koichi Yokozeki
yokozeki.4dg.kohichi@jp.nssmc.com

¹ Nippon Steel Corporation, Chiba, Japan

² Tokyo City University, Tokyo, Japan

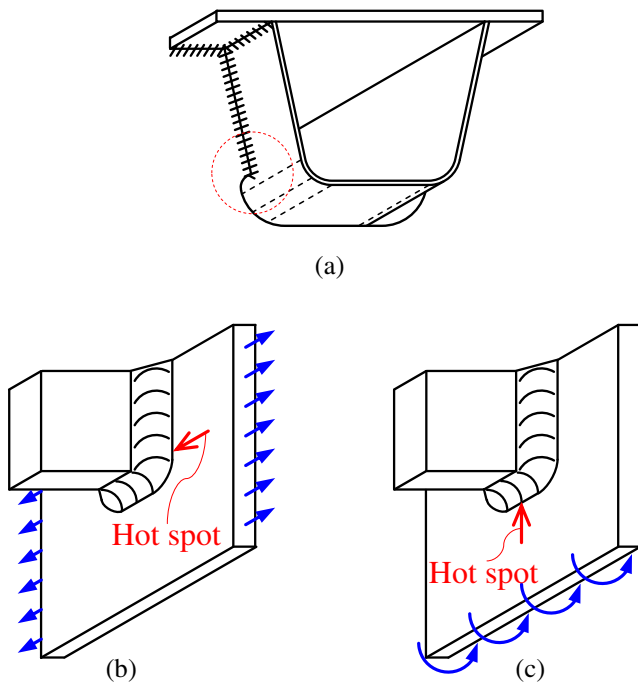
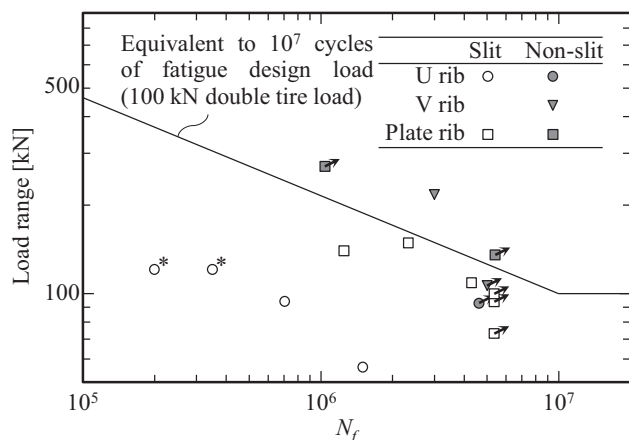


Fig. 1 Movement of the hot spot at the U-rib-to-transverse rib connection. **a** Connection between U rib and transverse rib. **b** Hot spot under in-plane tension. **c** Hot spot under out-of-plane bending

positions when assessing fatigue at longitudinal-to-transverse rib connections [16]. However, conventional fatigue designs and investigations regarding orthotropic steel decks have not yet sufficiently assessed the movement of hot spot locations or the complex influence surfaces that may appear.

For these reasons, the authors conducted fatigue assessments of various types of longitudinal-to-transverse rib connections while taking into account the stress generation mechanisms described above [17]. Figure 2 shows the relationships between the load ranges and the fatigue test results for longitudinal-to-



*Cracks observed from the weld roots of ribs to deck plate joints following testing using a single tire load (load ranges have been converted to double tire loads)

Fig. 2 The relationships between the load ranges and fatigue test results for various orthotropic steel deck designs

transverse rib connections, based on previous data [12, 17]. Such prior investigations demonstrated that non-slit connections (defined as those that do not have slits (cut-outs) on transverse rib webs during fabrication) exhibit high fatigue strengths compared to slit connections. However, previous studies did not analyze the effects of structural details on hot spot locations or on influence surfaces. Therefore, the work reported herein attempted to clarify the effects of both the rib shape and the presence of slits on hot spot locations and influence surfaces at longitudinal-to-transverse rib connections.

2 Computations of hot spot stresses associated with three-dimensionally deformed connections

2.1 Models of longitudinal-to-transverse rib connections

Six types of longitudinal-to-transverse rib connections (Table 1) were evaluated to clarify the effect of connection details on fatigue properties. U, V and plate longitudinal ribs and a transverse rib were assessed, together with slit and non-slit webs (Fig. 3). The U rib had a cross-section that is commonly employed in Japan, while the cross-section of the V rib had a V shape with the same radius as in the bending plate process and approximately the same cross-sectional area as the U rib. The cross-section of the plate rib was given approximately the same sectional modulus as a commonly used bulb rib with a height of 230 mm height and a thickness of 11 mm, taking the effective width of the deck plates into account for the cross-sections. The slit details for connections US and PS were determined based on standard recommendations [18], while the slit radius of connection PS was enlarged to 45 mm, since recent research has shown that this can improve fatigue strength [4]. The slit dimensions for connection VS were set such that the radius was the same as that for connection US. The arrows in Fig. 3 show the weld toes that were evaluated when assessing the fatigue at the connections. The presence of a greater number of arrows along the weld toe lines indicates that a hot spot is located somewhere along the weld toe line. In the following text, the weld toes are referred to using the connection name combined with the weld toe number. As an example, US-2 indicates weld toe 2 of connection US.

The hot spot stresses of the connections were computed using models with three or more longitudinal ribs and three or four transverse ribs (Fig. 4). The deformation of these structural members was considered when evaluating the stress conditions at the longitudinal-to-transverse rib connections [8]. It should be noted that it is difficult to obtain the appropriate stress conditions at longitudinal-to-transverse rib connections when using smaller models, such as those with only one transverse

Table 1 The connections evaluated in this study

Connection	Longitudinal rib			Slit	Deck plate thickness (mm)
	Type	Thickness (mm)	Span (mm)		
US	U	6	2500	Slit	16
UN	U	6	2500	Non-slit	16
VS	V	6	2500	Slit	16
VN	V	6	2500	Non-slit	16
PS	Plate	16	1667	Slit	12
PN	Plate	16	1667	Non-slit	12

rib. The connections that were evaluated in these models represented the intersections between the center longitudinal rib and the center transverse rib. Longitudinal ribs adjacent to main girders were not evaluated since their deformations could be significantly affected by boundary conditions at the deck plate ends supported by main girders.

The longitudinal rib span lengths in the models were set based on the typical lengths of actual structures in Japan. Inner diaphragms for protection against corrosion were considered to be installed in the models for connections US, UN, VS, and VN to simulate actual structural conditions, since such diaphragms can increase stresses at longitudinal-to-transverse rib connections [19]. The weld leg length was set at 6 mm, except in the case of joints positioned between plate ribs and the non-slit transverse rib, for which the value was 8 mm. This increased length was necessary to maintain adequate weld throats in conjunction with the enlarged 2-mm weld root gaps and to ensure efficient assembly of connection PN. Although surfacing has been found to affect stresses in orthotropic steel

decks, surfacing was neglected in this study due to the uncertainty of the resulting mechanical properties inputs during the finite element analyses. Surfacing would be expected to decrease the stresses in orthotropic steel decks up to a certain temperature [20], and so models without surfacing will provide safer fatigue evaluations.

2.2 Loads and boundary conditions

Figure 5 shows the load model and the positions employed for stress analyses. The load was simulated by applying a uniformly distributed pressure with a total force of 100 kN on the load area to simulate a double tire, as shown in Fig. 5a. These parameters were selected based on a fatigue design load (T load) specified in the Specification for Highway Bridges [18]. A T load is based on a single axle model that simplifies the rear tandem axle of a truck. This study used the simplified load model to elucidate the relationship between load positions and hot spot stresses at evaluated connections. The load

Fig. 3 Evaluated longitudinal-to-transverse rib connections and weld toes. **a** Connection US. **b** Connection UN. **c** Connection VS. **d** Connection VN. **e** Connection PS. **f** Connection PN

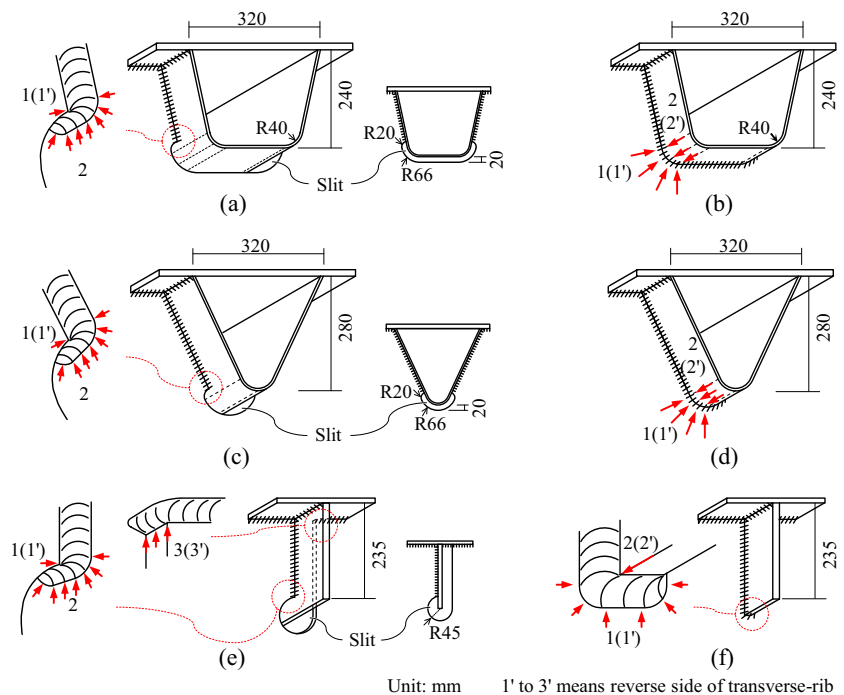
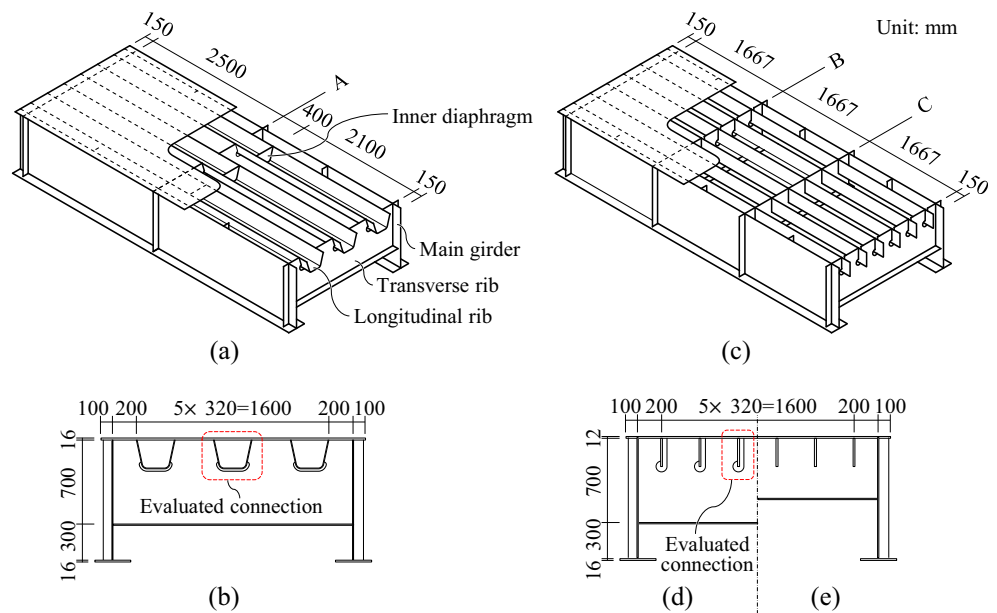


Fig. 4 The longitudinal-to-transverse rib connections and weld toes evaluated in this study. **a** The model for connection US (note that the models for connection UN, VS and VN had the same dimensions except for the rib and slit shape). **b** Cross-section A. **c** The model for connections PS and PN. **d** Cross-section B (connection PS). **e** Cross-section C (connection PN)



position, meaning the center of the double tire load, was moved in both the longitudinal and transverse directions as shown in Fig. 5. The transverse spacing of the load positions was set to 160 mm, which is half the longitudinal rib spacing. The longitudinal spacing was set to 200 mm for the U and V ribs and 100 mm for the plate rib. A load position with a relatively finer mesh was applied to the plate rib since local stresses at the connection with the plate rib were expected to be more sensitive to the load position. The boundary conditions were the vertical supports at both ends of the main girder flanges to simulate deflection of the main girders. The ends of the flanges were also supported horizontally to simplify the girder condition.

2.3 Finite element analyses parameters

Elastic finite element analyses were conducted using the Abaqus 6.13 software package. In these calculations, the finite element models were composed of four-node shell elements (Fig. 6a) and the elastic modulus and Poisson’s ratio of the steel were 205 kN/mm² and 0.3, respectively. The sizes,

shapes and applied thicknesses of the shell elements around the hot spots were adjusted to allow computation of the stress concentrations at the welded joints. The elements were primarily rectangles with sizes equal to or smaller than 0.2 times the plate thicknesses (Fig. 6b). In the case that hot spots were situated at the plate edge, the element sizes were set to 2 mm. In addition, the thicknesses at the welded joints were increased to simulate increased stiffness, based on prior research [21]. The other parts of models were based on meshes with relatively coarse sizes up to 100 mm. Because only the parts being evaluated were modeled with fine meshes, the models for connections PS and PN had different meshes even though both models were geometrically identical.

2.4 Hot spot stress computation procedures

Hot spot stresses were computed as structural stresses based on extrapolations that took thickness and bending effects into account as detailed in a previous study [17], using the following equation.

Fig. 5 Load conditions. **a** Loads for connections US, UN VS and VN. **b** Loads for connections PS and PN

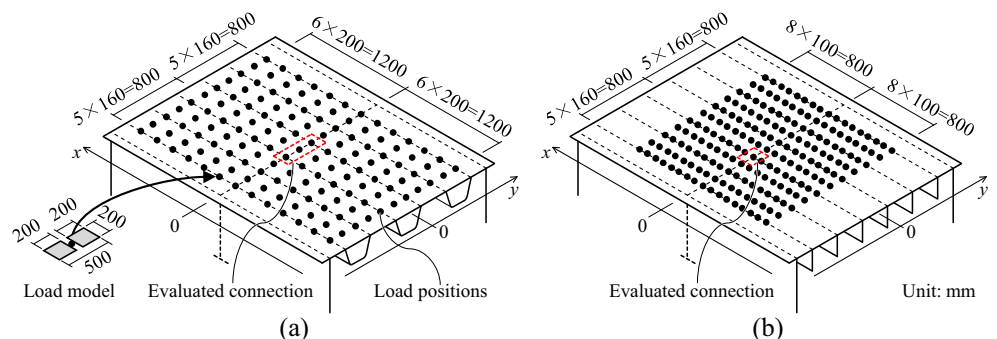
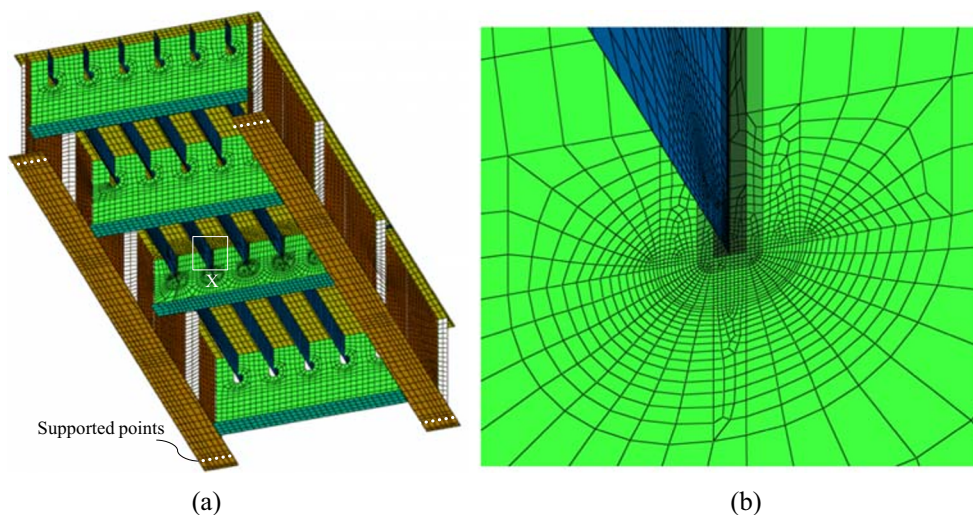


Fig. 6 Finite element model. **a** Overall view. **b** Welded joints between longitudinal and transverse ribs in the region labeled X in (a)



$$\sigma'_h = (t/25)^{0.25} (\sigma_{h,m} + 0.8\sigma_{h,b}) \tag{1a}$$

$$\sigma_{h,m} = (\sigma_{h,obv} + \sigma_{h,rev})/2 \tag{1b}$$

$$\sigma_{h,b} = (\sigma_{h,obv} - \sigma_{h,rev})/2 \tag{1c}$$

Here σ'_h is the factored hot spot stress while $\sigma_{h,m}$ and $\sigma_{h,b}$ are the membrane and out-of-plane bending components of the hot spot stress, respectively, and $\sigma_{h,obv}$ and $\sigma_{h,rev}$ are the hot spot stresses for the obverse and reverse surfaces being evaluated, respectively. The hot spot stresses based on surface stresses were calculated from the following equation [22].

$$\sigma_h = \begin{cases} 1.67\sigma_{0.4t} - 0.67\sigma_{1.0t} & (2a) \\ 3\sigma_{4\text{ mm}} - 3\sigma_{8\text{ mm}} + \sigma_{12\text{ mm}} & (2b) \end{cases}$$

Here, the σ term on the right side of the equation is the surface stress perpendicular to the weld toe lines and the subscripts to this term indicate the distances from the weld toes to the stress reference points. Equations 2a and 2b are applied when determining hot spot stresses at plate surfaces and edges, respectively.

The weld toe lines examined in this work were not points but rather lines and hot spots moved along these lines as the load position and hence the principal stress direction changed (Fig. 1). This migration of hot spots could be reproduced in the finite element analysis. In such cases, the weld toe lines were composed of several nodes and those nodes at which the maximum and minimum weld toe stresses appeared varied as the load position moved (Fig. 7). To take this movement into account, maximum and minimum hot spot stresses were searched for along the weld toe line after the hot spot stresses of all nodes in the welded toe are calculated by Eq. 1. The stresses were determined via numerical expressions by setting $pos = 1 - n$ for the load cases and $node = 1 - m$ for the node numbers comprising the evaluated weld toe lines. Subsequently, the hot spot

stress at each node for each load case could be expressed as in the following equation.

$$\sigma'_{h,pos,node} = \begin{cases} \sigma'_{h,1,1}, \sigma'_{h,1,2}, \dots, \sigma'_{h,1,m}, \\ \sigma'_{h,2,1}, \sigma'_{h,2,2}, \dots, \sigma'_{h,2,m}, \\ \vdots \\ \sigma'_{h,n,1}, \sigma'_{h,n,2}, \dots, \sigma'_{h,n,m} \end{cases} \tag{3}$$

In addition, the maximum and minimum hot spot stresses along the weld toe line ($\sigma'_{h,pos,u}$ and $\sigma'_{h,pos,b}$) could be expressed as in the following equation.

$$\sigma'_{h,pos,u} = \max(\sigma'_{h,pos,1}, \sigma'_{h,pos,2}, \dots, \sigma'_{h,pos,m}) \tag{4a}$$

$$\sigma'_{h,pos,b} = \min(\sigma'_{h,pos,1}, \sigma'_{h,pos,2}, \dots, \sigma'_{h,pos,m}) \tag{4b}$$

$$pos = 1, 2, \dots, n \tag{4c}$$

After iterating the procedure to determine $\sigma'_{h,pos,u}$ and $\sigma'_{h,pos,b}$ for all load cases, the maximum and minimum hot spot stresses ($\sigma'_{h,max}$ and $\sigma'_{h,min}$) and the hot spot stress ranges ($\Delta\sigma'_h$) for the weld toes caused by the moving load were calculated using the following equation.

$$\sigma'_{h,max} = \max(\sigma'_{h,1,u}, \sigma'_{h,2,u}, \dots, \sigma'_{h,n,u}) \tag{5a}$$

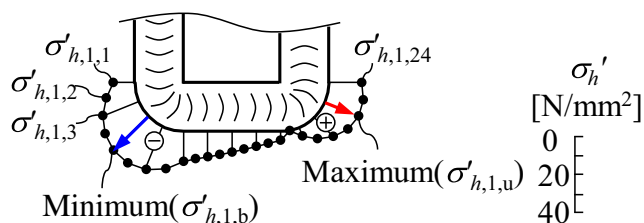


Fig. 7 An example of stress distribution along the weld toe

$$\sigma'_{h,\min} = \min(\sigma'_{h,1,b}, \sigma'_{h,2,b}, \dots, \sigma'_{h,n,b}) \quad (5b)$$

$$\Delta\sigma'_h = \sigma'_{h,\max} - \sigma'_{h,\min} \quad (5c)$$

In contrast, the hot spot stress ranges for each node were determined via the equation below.

$$\sigma'_{h,\max,node} = \max(\sigma'_{h,1,node}, \sigma'_{h,2,node}, \dots, \sigma'_{h,n,node}) \quad (6a)$$

$$\sigma'_{h,\min,node} = \min(\sigma'_{h,1,node}, \sigma'_{h,2,node}, \dots, \sigma'_{h,n,node}) \quad (6b)$$

$$\Delta\sigma'_{h,node} = \sigma'_{h,\max,node} - \sigma'_{h,\min,node} \quad (6c)$$

$$node = 1, 2, \dots, m$$

It should be noted that the hot spot stress ranges calculated with Eq. 5c could be greater than those obtained from Eq. 6c. However, it is not yet known whether Eq. 5c or Eq. 6c is more appropriate for fatigue evaluation, and so Eq. 5c is employed so as to err on the side of caution in this study.

3 Hot spot locations

Figure 8 presents the $\sigma'_{h,\max}$, $\sigma'_{h,\min}$ and mean stress values (that is, the averages of $\sigma'_{h,\min}$ and $\sigma'_{h,\max}$) for the evaluated weld toes. Because the hot spot stress range of weld toe US-2 was larger than that of US-1, US-2 was selected as a representative weld toe for analysis in this section using model 1. In the same manner, VS-2, UN-2, and VN-2 were selected for analysis. In the PS and PN models, although weld toes PS-3 and PN-2 had the largest hot spot stress ranges, they were located at plate edges and comprised only one node. Therefore, weld toes PS-2 and PN-1 were analyzed instead. Note that, in the following text, the phrase “hot spot” indicates the node at which $\sigma'_{h,pos,u}$ and $\sigma'_{h,pos,b}$ appeared in each of the weld toes.

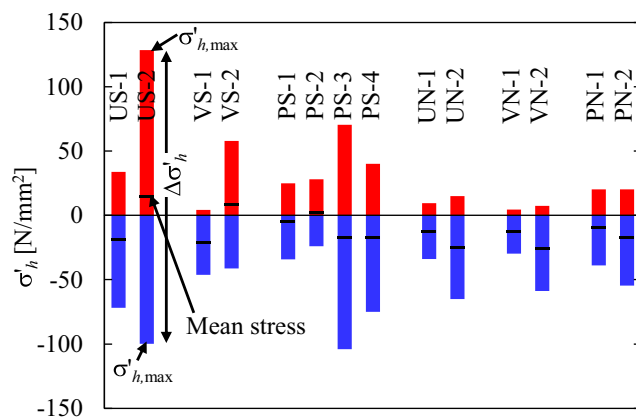
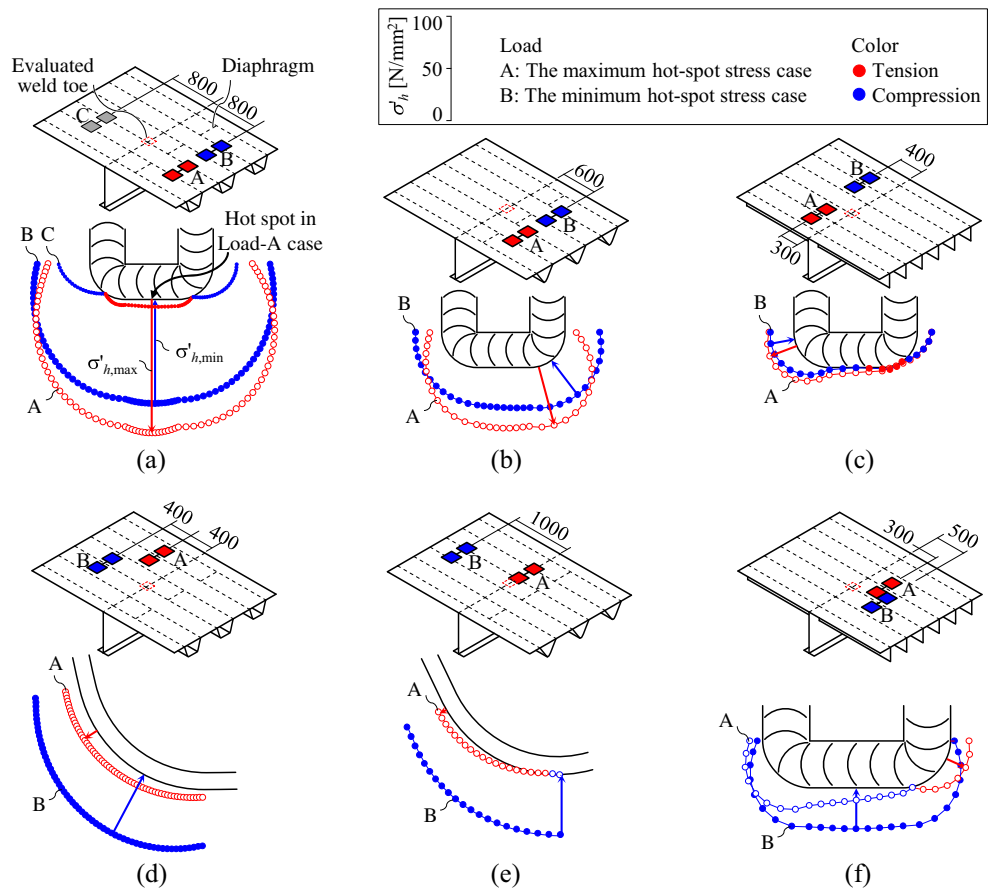


Fig. 8 The maximum and the minimum hot spot stresses ($\sigma'_{h,\max}$ and $\sigma'_{h,\min}$) and mean stresses of evaluated weld toes

Figure 9 shows the hot spot stress distributions along the weld toes for the loads that produced $\sigma'_{h,\max}$ and $\sigma'_{h,\min}$ at the evaluated weld toes (hereinafter termed load A and load B, respectively). The hot spot locations along the weld toes were moved as the load position moved and these locations were different between load A to load B for each of the box weld toe lines assessed, with the exception of US-2. The hot spots for weld toe US-2 were situated at the bottom center of the box weld in conjunction with both $\sigma'_{h,\max}$ and $\sigma'_{h,\min}$ (Fig. 9a) and the hot spot for this same weld toe also migrated to the side of the box weld for load case C (Fig. 9). The hot spots for weld toes VS-2, PS-2 and PN-1 were located at the corners of the box welds for both load A and load B (Fig. 9b, c and e). Figure 10 provides the ratios of the hot spot stress ranges of the nodes ($\Delta\sigma'_{h,node}$) to the hot spot stress ranges of the weld toes ($\Delta\sigma'_h$). $\Delta\sigma'_{h,node}$ was calculated using Eq. 6 with the evaluation points fixed at the side, the bottom and the corner of each weld. The hot spot stress ranges calculated for fixed evaluation points were evidently smaller than those calculated using Eq. 5 (that is, $\Delta\sigma'_h$) for all cases shown in Fig. 10, except for weld toe US-2. Therefore, a fatigue evaluation based on hot spot stresses obtained from fixed evaluation points can potentially be inaccurate in terms of finding the maximum hot spot stress ranges.

The hot spot stress ranges at the base of each of weld toes US-2 and VS-2 were 100% and 97% of $\Delta\sigma'_h$, respectively (Fig. 10). In addition, the out-of-plane bending stress components ($0.8\Delta\sigma'_{h,b}$) accounted for 88% and 72% of the hot spot stress ranges for these same two weld toes. Therefore, out-of-plane bending of the walls of the U rib and the V rib about the longitudinal axis, as shown in Fig. 1c, could be the dominant deformation. The hot spot stress range at the side of PS-2 was 91% of $\Delta\sigma'_h$ while the bending stress component accounted for 96% of the range. Thus, out-of-plane bending of the plate rib about the vertical axis was the dominant effect for this weld toe. The hot spot stress ranges at the side and base of weld toe PN-1 were only 51% and 70% of the hot spot stress range, respectively. This result shows that the hot spot locations were different between the corner and the base of the box weld toe when $\sigma'_{h,\max}$ and $\sigma'_{h,\min}$ appeared (Fig. 9e). These results confirm that the hot spot locations varied depending on the structural details. Although the slit connections showed the same behavior in which out-of-plane bending was dominant during stress, the hot spot locations were different and were dependent on the longitudinal rib shapes. Such differences are thought to result from variations in the direction of the out-of-plane bending. The hot spot locations of the non-slit connections were also found to vary depending on the longitudinal rib shapes. Therefore, it is important to determine the situation of hot spots along the weld toes when conducting fatigue assessments of longitudinal-to-transverse rib connections.

Fig. 9 Hot spot locations and stress distributions along the weld toes. **a** Weld toe US-2. **b** Weld toe VS-2. **c** Weld toe PS-2. **d** Weld toe UN-2'. **e** Weld toe VN-2. **f** Weld toe PN-1



4 Relationships between load positions and hot spot stresses

Figure 11 presents the influence surfaces using plots in which the x and y axes equate to the load positions, using contour means showing the largest absolute values of $\sigma'_{h,pos,u}$ and $\sigma'_{h,pos,b}$ for the weld toes. Each weld toe in Fig. 11 had the

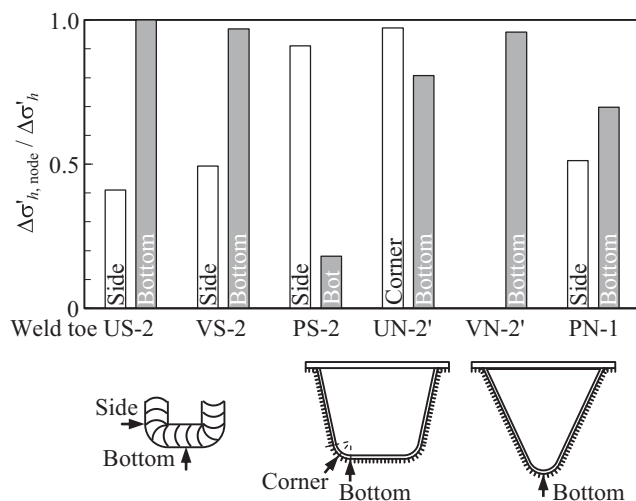
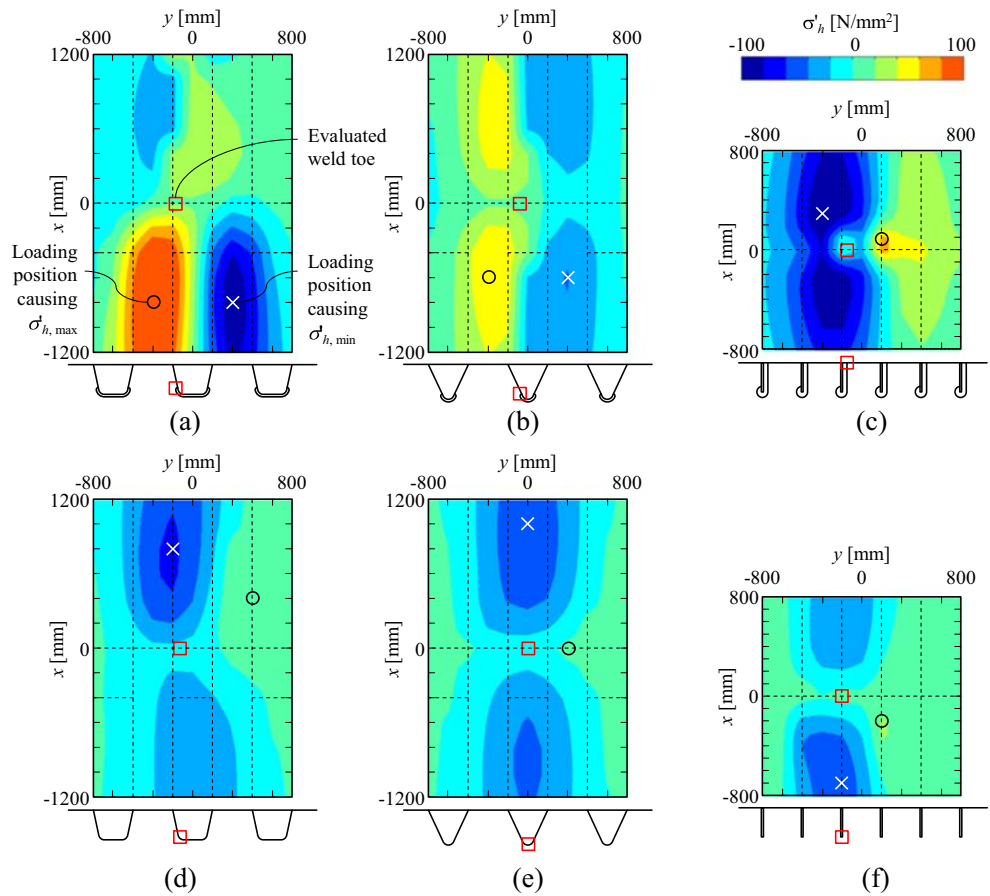


Fig. 10 Ratios of hot spot stress ranges of nodes ($\Delta\sigma'_{h,node}$) to hot spot stress ranges of weld toes ($\Delta\sigma'_h$)

largest hot spot stress range ($\Delta\sigma'_h$) among the various weld toes in each model. The load positions associated with $\sigma'_{h,max}$ and $\sigma'_{h,min}$ (hereinafter termed POS_{max} and POS_{min} , respectively) for each weld toe are also indicated in Fig. 11 by circle and cross marks, respectively. It is evident that the POS_{max} and POS_{min} for the weld toes having slit connections as well as for connection UN were not on the center axes of the longitudinal or transverse ribs but rather some distance away from the centers of the evaluated connections in both the longitudinal and transverse directions (Fig. 11a–d). Eccentric load positions such as these were also observed in a previous study with U and plate ribs [13, 14, 16]. Furthermore, POS_{max} and POS_{min} were situated in different lanes. As an example, POS_{max} and POS_{min} for weld toe US-2 were located at $(x, y) = (-800, -320 \text{ mm})$ and $(-800, +320 \text{ mm})$, respectively. The locations of POS_{max} and POS_{min} in lanes distant from the center axes of the longitudinal ribs could have resulted from out-of-plane bending stresses at weld toe US-2 (induced by the rotational deformation of the U rib), stresses at weld toe UN-2' (induced by the distortion of the U rib) and stresses at weld toe PS-3' (induced by the shear deformation of the transverse rib webs) [14].

In contrast, in the case of the influence surfaces for weld toes VN-2' and PN-2, POS_{min} was located on the center axes of the longitudinal ribs while POS_{max} and POS_{min}

Fig. 11 Relationships between load positions and hot spot stresses (influence surfaces). **a** Influence surface of weld toe US-2. **b** Influence surface of weld toe VS-2. **c** Influence surface of weld toe PS-3'. **d** Influence surface of weld toe UN-2'. **e** Influence surface of weld toe VN-2'. **f** Influence surface of weld toe PN-2



were located in different lanes, as was observed for the other connections. The observation that the POS_{max} and POS_{min} were situated in different lanes indicates that hot spot stress ranges associated with longitudinal-to-transverse rib connections in bridges during use cannot be simulated by fatigue tests based on cyclic design loads at fixed positions or fixed lanes. The latter two types of tests correspond to constant amplitude and running wheel fatigue tests, respectively. As an example, a constant amplitude fatigue test for weld toe US-2 with a load range, P , at the POS_{max} for this weld toe would generate only 56% of the hot spot stress range caused by a moving load with weight P according to the analysis results.

Figure 12 summarizes the relationships between the transverse distances from rib centers to load centers and the ratios of the out-of-plane bending components for the hot spot stresses in conjunction with the maximum and minimum hot spot stresses. These data are based on the same weld toes as in Fig. 11. It should be noted that the evaluated weld toes were longitudinal rib side weld toes of welded joints between longitudinal and transverse ribs, with the exception of PS-3', which was a transverse rib side weld toe of welded joints between the transverse rib and the deck plate.

The bending component tended to increase as the transverse distance from the rib center to the load center increased,

and the ratios of the bending components were from 0.64 to 0.98 for the weld toes of the slit connections. A large contribution of out-of-plane bending to the local stress at connection US was also observed in a prior field study [13]. As confirmed by Fig. 11, the load centers were transversely distant from the rib centers in the case of the slit connections. However, the ratios of the bending components were below 0.5 in the weld toes of the non-slit connections, except for the $\sigma'_{h,max}$ of PN-2. From these results, it is probable that the POS_{max} and POS_{min}

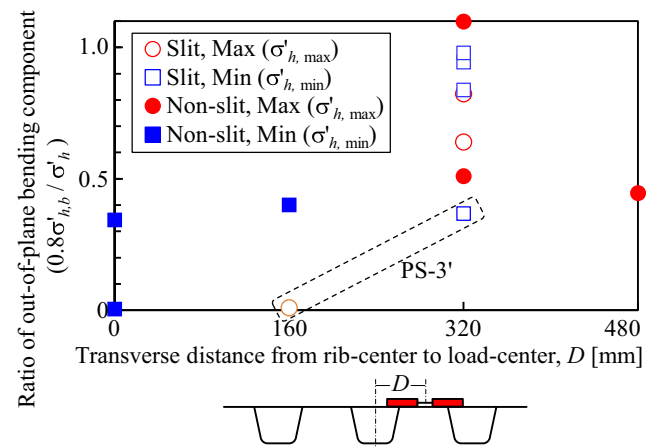


Fig. 12 Relationships between transverse distances from rib centers to load centers and ratios of out-of-plane bending components of hot spot stresses

were transversely removed from the longitudinal rib center because of the out-of-plane bending of the plates at the slit ends caused by eccentric loadings, which represented the primary local stress at the slit connections. Even so, it should be noted that these data were obtained from a limited number of finite elements models with some parameters fixed. In particular, the stiffness of the deck plate can affect the extent of deformation of both the longitudinal and transverse ribs. Therefore, thicker deck plates or deck plates with stiff pavements could give different results.

5 Conclusions

This study investigated the effects of rib shape and the presence of slits on the fatigue properties of longitudinal-to-transverse rib connections. Both slit and non-slit connections with U ribs, V ribs and plate ribs were assessed while considering the movement of hot spot locations along weld toes in response to moving loads. The exception was that migration of hot spots was not considered when the weld toes being evaluated were at plate edges. The following conclusions were obtained.

1. The hot spot locations along weld toes were different depending on both the longitudinal rib shape and whether or not slits were present. The hot spot locations also varied between the case of the load causing the maximum hot spot stress and the case of the load causing the minimum hot spot stress for each of the evaluated weld toe lines except for weld toe US-2. Therefore, a fatigue evaluation using hot spot stresses with fixed evaluation points could potentially provide inaccurate maximum hot spot stress ranges.
2. The load positions causing the maximum and minimum hot spot stresses on the slit connections tended to be some distance away from the center axes of the evaluated ribs. The bending components of the hot spot stresses were also found to increase as the distances increased transversely. In contrast, the load positions producing the minimum hot spot stresses at the non-slit connections were located on the center axes of the longitudinal ribs being assessed.

Funding This work was supported by IHI Infrastructure Systems Co., Ltd., JFE Engineering Corporation, JFE Steel Corporation, Kawada Industries, Inc., Kobe Steel, Ltd., Komaihaltec, Inc., Mitsui Zosen Steel Structures Engineering Co., Ltd., Miyaji Engineering Co., Ltd., MM Bridge Co., Ltd., Nippon Steel & Sumitomo Metal Corporation and Yokogawa Bridge Corp.

References

1. Wolchuk R (1987) Application of orthotropic decks in bridge rehabilitation. *Eng J (AISC)* 24(3):113–121
2. de Jong FBP (2004) Overview fatigue phenomenon in orthotropic bridge decks in the Netherlands. *Proc 1st Int Orthotropic Bridge Conf*, Aug. 23–27, Sacramento: 489–512
3. Yuge T, Machida F, Morikawa H, Miki C, Kamiki T, Matsui T (2004) Analysis of fatigue damage patterns in orthotropic steel deck of Tokyo Metropolitan Expressway. *Proc 1st Int Orthotropic Bridge Conf*, Aug. 23–27, Sacramento: 531–542
4. Subcommittee on Fatigue of Orthotropic Steel Bridge Deck (2011) *Fatigue of Orthotropic Steel Deck*. Maruzen, Tokyo
5. Gurney T (1992) *Fatigue of steel bridge decks*. HMSO, London
6. Fryba L, Gajdos L (1999) Fatigue properties of orthotropic decks on railway bridges. *Eng Struct* 21(7):639–652
7. Taskopoulos P, Fisher JW (2003) Full-scale fatigue tests of steel orthotropic decks for the Williamsburg Bridge. *J Bridge Eng (ASCE)* 8(5):323–333
8. Miki C, Suganuma H (2014) Rehabilitation of strengthening of orthotropic steel bridge decks. In: Chen WF, Duan L (eds) *Bridge engineering handbook*, second edition: construction and maintenance. CRC Press, Boca Raton
9. Miki C, Tateishi K, Takagi S (1991) Field stress measurements at the connection between longitudinal and transverse ribs of steel deck plates. *J Struct Eng A (JSCE)* 37(3):1163–1168
10. Lehrke HP (1997) Measurements and interpretation of dynamic loads on bridges, Final report. Commissions of European Committees, EUR 16851, Brussels
11. Delesie C, Bogert PV (2008) The effect of stiffener distortion of orthotropic steel bridge decks on load dispersal behavior and stress concentrations. *Proc 2nd Int Orthotropic Bridge Conf*, Aug. 25–29, Sacramento: 306–326
12. Yokozeki K, Miki C (2016) Fatigue evaluation for longitudinal-to-transverse rib connection of orthotropic steel deck by using structural hot spot stress. *Weld World* 60(1):83–92
13. Miki C, Tateishi K, Okukawa A, Fujii Y (1995) Local stress and fatigue strength of the joint between longitudinal and transverse ribs in orthotropic steel deck plate. *J JSCE* 519:127–137
14. Yokozeki K, Yokoyama Y, Tominaga T, Miki C (2017) Fatigue enhancement of longitudinal-to-transverse rib connection in orthotropic steel deck. *J JSCE Ser A1* 73(1):206–2017
15. Leonard DR (1972) A traffic loading and its use in the fatigue life assessment of highway bridges. TRRL Report, LR252
16. Yan F, Chen W, Lin Z (2016) Prediction of fatigue life of welded details in cable-stayed orthotropic steel deck bridges. *Eng Struct* 127:344–358
17. Yokozeki K, Miki C (2017) Fatigue assessment of various types of longitudinal-to-transverse rib connection in orthotropic steel decks. *Weld World* 61(3):539–550
18. Japan Road Association (2014) Specification for highway bridges (ver. 2014), Part2 steel bridges. Maruzen, Tokyo
19. Hanji T, Kato K, Tateishi K, Choi S, Hirayama S (2013) Local stress characteristics at cross-beam web cutout in closed rib orthotropic deck. *Proc. 3rd Int. Orthotropic Bridge Conf.*, Jun. 24–30, Sacramento: 262–277
20. Cheng X, Murakoshi J, Nishikawa K, Ohashi H (2004) Local stresses and fatigue durability of asphalt paved orthotropic steel decks. *Proc. 1st Int Orthotropic Steel Bridge Conf*, Aug. 25–27, Sacramento: 543–555
21. Machida S, Matoba M, Yoshinari H, Nishimura R (1992) Definition of hot spot stress in welded structure for fatigue assessment (3rd Report). *J Soc Naval Architects Jpn* 171:477–484
22. Hobbacher A (2009) Recommendations for fatigue design of welded joints and components. *Welding Research Council Inc.*, New York

Publisher's note Springer Nature remains neutral with regard to jurisdictional claims in published maps and institutional affiliations.